Heterogeneous individual motility biases group composition in a model of aggregating cells

Mathieu Forget[a,b], Sandrine Adiba[a], Leonardo Gregory Brunnet[c], Silvia De Monte[a,b]

[a] *Institut de Biologie de l'ENS (IBENS), Département de biologie, Ecole normale supérieure, CNRS, INSERM, Université PSL, 75005 Paris, France*
[b] *Department of Evolutionary Theory, Max Planck Institute for Evolutionary Biology, Plön, Germany*
[c] *Theoretical and Computational Modeling Group, Physics Institute, Federal University of Rio Grande do Sul, Porto Alegre, Brazil*

Supplementary Figures

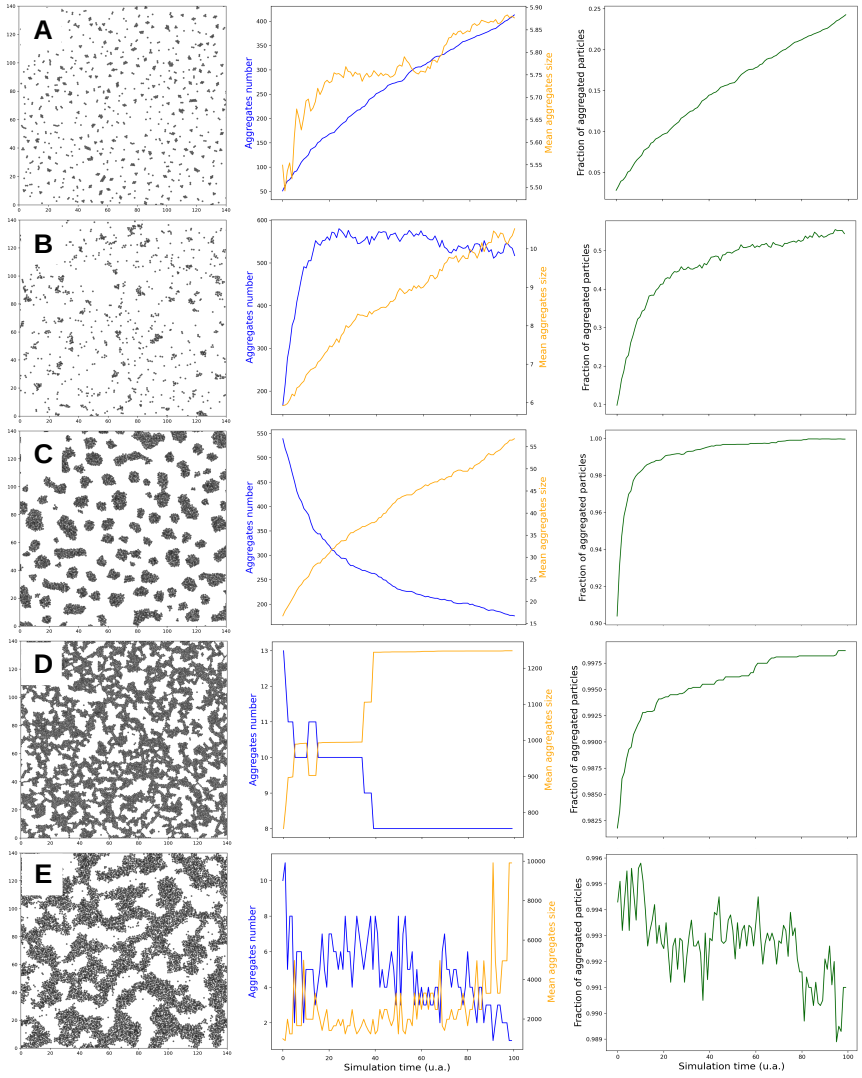

Figure S1: **Variation in particle speed and packing fraction produces different aggregation dynamics.** Snapshots of the final state (first column) of the system and evolution of aggregate number and aggregate mean size (second column), as well as the fraction of aggregated particles over time (third column), for simulations ran using the 5 pairs of parameters values displayed in Fig. 2 (**A**: $v_0 = 2.5$, $\rho = 0.05$, **B**: $v_0 = 17.5$, $\rho = 0.05$, **C**: $v_0 = 12$, $\rho = 0.2$, **D**: $v_0 = 2.5$, $\rho = 0.35$ and **E**: $v_0 = 17.5$, $\rho = 0.35$). The five different regimes discussed in the text correspond to different variations of the three order parameters.

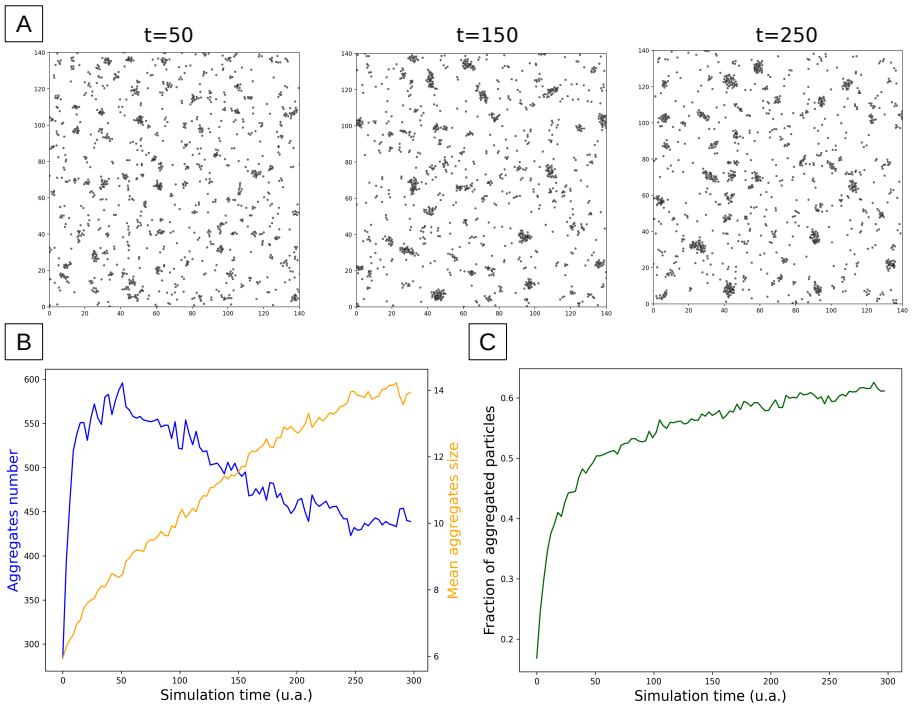

Figure S2: **Aggregates' long-term coarsening dynamics at high speed and small packing fraction**. During the time span $t_f = 100$, self-organization of fast particles leads to the rapid formation of a large number of small aggregates. On longer timescales, however, particles evaporate from small and unstable aggregates and attach to larger-size aggregates that are more stable (**A**, snapshots of the system state at $t = 50$, $t = 150$ and $t = 250$). Similarly to Ostwald's ripening processes (Ostwald, 1896), this results in a decrease in the number of aggregates (**B**). The fraction of aggregated particles (**C**) saturates at a value smaller than 1, indicating that in the asymptotic state the aggregated phase coexists with the gas phase, as in MIPS (Fily and Marchetti, 2012). In this simulation, $\rho = 0.07$, $v_0 = 17.5$, and other parameters were set as indicated in table 1.

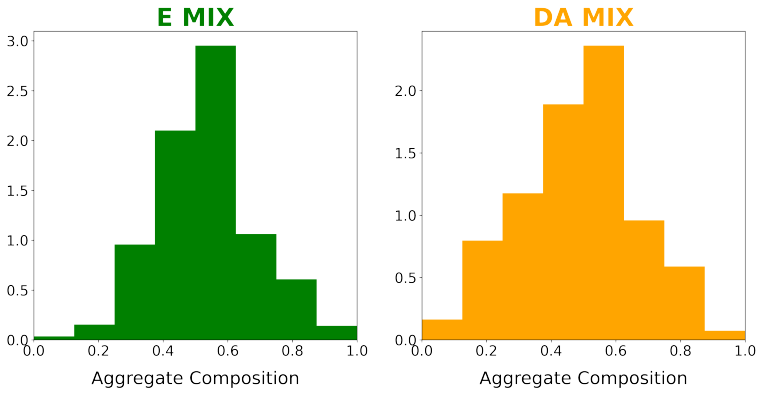

Figure S3: **Distribution of aggregates composition for simulations ran with two types of binary mixes**. Aggregate composition was measured in the two binary mixes presented in Fig. 3A (DA and E mix). The packing fraction was fixed to 0.07 and the remaining parameters of the model were set as indicated in table 1. In both cases, the distribution of aggregate composition is unimodal, indicating that heterogeneity in particles motility does not induce segregation of the two types in different aggregates.

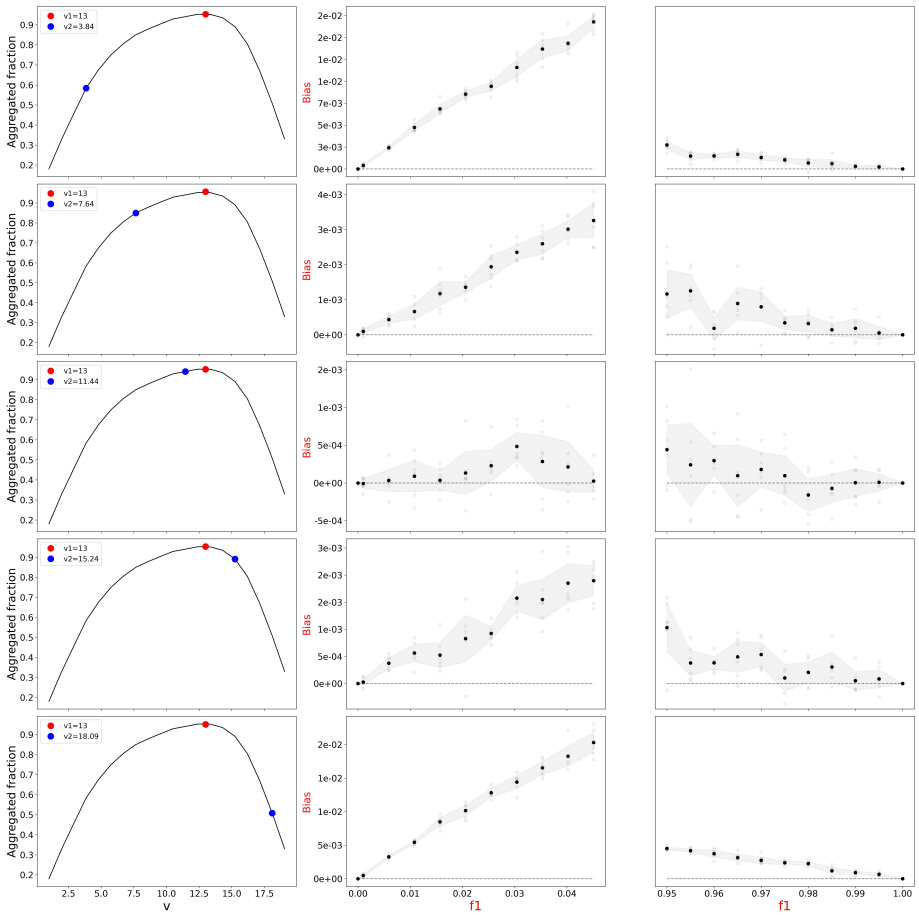

Figure S4: **Bias in binary mixes where the focal population has constant speed, and speed differential varies.** The first column displays the fraction of aggregated particles when each population aggregates separately at the same total packing fraction $\rho = 0.07$ (other parameters were set as indicated in table 1. Red dots indicate the constant speed $v_1 = 13$ of the focal population, blue dots the speed v_2. The second and third column illustrate the bias relative to the focal population at the extremes of the interval $[0, 1]$. Black dots are averages of six replicates, the shaded area represents the 95% confidence interval.

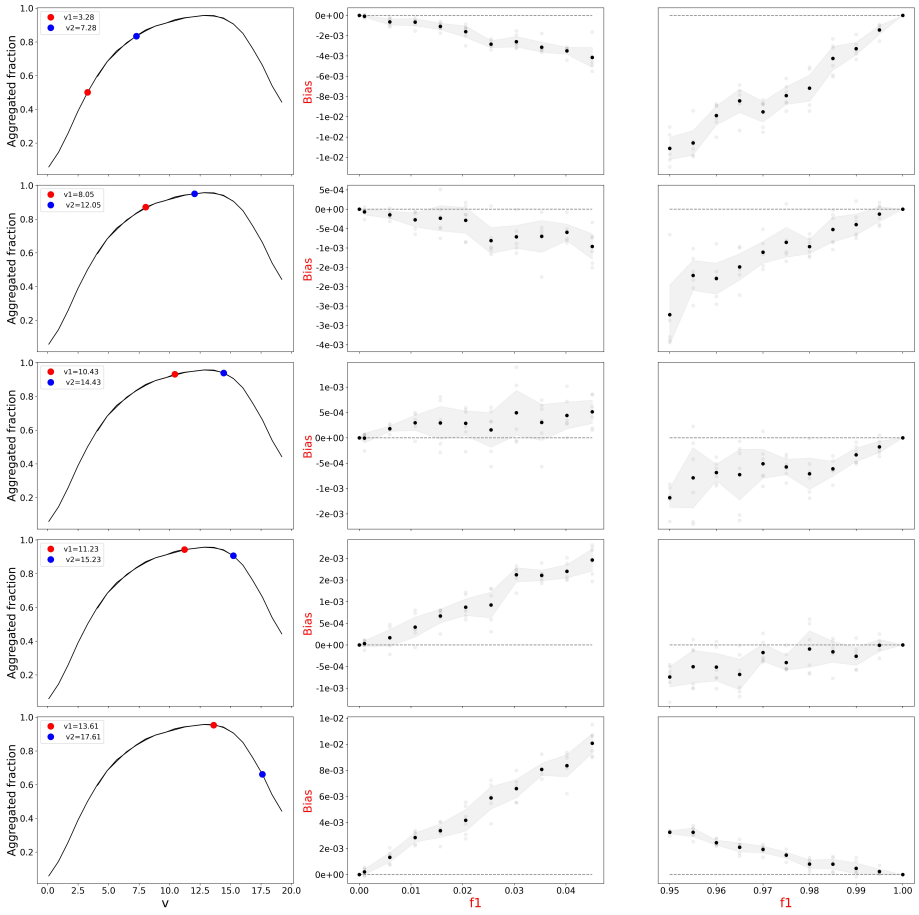

Figure S5: **Bias in binary mixes where the speed of the two populations is changed, while maintaining a fixed speed differential.** The first column displays the fraction of aggregated particles when each population aggregates separately at the same total packing fraction $\rho = 0.07$ (other parameters were set as indicated in table 1). Red dots indicate the speed v_1 of the slower, focal population, blue dots the speed v_2, chosen such that the speed difference $\Delta v = 4$. The second and third column illustrate the bias relative to the focal, slower population at the extremes of the interval $[0, 1]$. Black dots are averages of six replicates, the shaded area represents the 95% confidence interval.

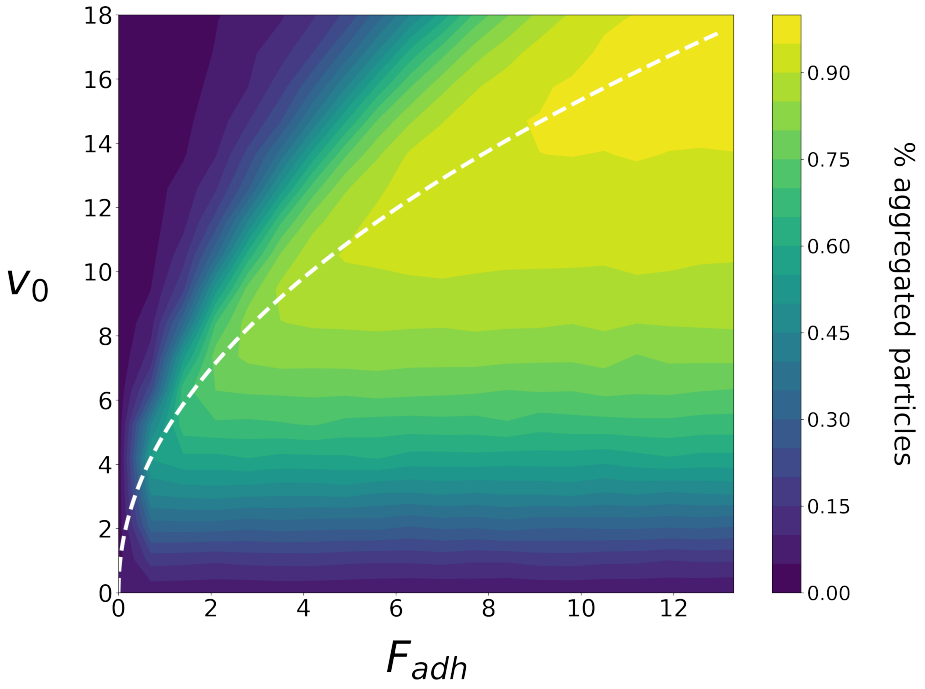

Figure S6: **Fraction of aggregated particles at the end of the simulation as a function of particles adhesive strength and particle speed**. The packing fraction was fixed to 0.07 and the remaining parameters of the model were set as indicated in table 1. The white dotted line represents a fit of the points corresponding to the highest fraction of aggregated particles.

Supplementary Information

Parameters choice

The fixed parameters of the model were set as indicated in table 1. As in Szabo et al. (Szabó et al., 2006), we used a fixed time step dt of $dt = 0.05 * R_0/v_0 = 0.01$. This value is sufficiently small so that, between two successive time-steps, two particles cannot cross each other's interaction range without interacting.

The interaction parameters F_{rep} and F_{adh} were set so that particles do not collapse (volume exclusion) and can detach from aggregates (evaporation) when v_0 is increased. The equilibrium radius R_{eq} and the interaction range R_0 are such that particles only interact with their direct neighbours, in order to model cell interaction through physical contact. Interactions mediated by diffusing signals could be approximated by choosing larger radii, but that would require making additional assumption on signal take-up by neighbouring cells. The intensity of angular noise η and the relaxation time of interaction τ were set such that particles clusters do not display collective motion, similar to what can be observed during early aggregation of *Dictyostelium discoideum*. Indeed, a low level of angular noise and/or a low relaxation time favor collective motion of particles as interactions contribute to aligning the self-propelled velocity and nematic order emerges. Moreover, we chose a relatively high value of η so that, in the absence of particles interaction, the trajectory of a particle resembles that of a starved *D. discoideum* cells in the absence of interaction with other cells, *i.e.* at low cell density (See Fig. 1C and D for a comparison).

Other parameters were set to match the order of magnitude of observations of *D. discoideum* under standard laboratory conditions: cell size $R_{eq}^{exp} = 11\mu m$ (De Palo et al., 2017), cell speed $v^{exp} = 11\mu m/min$ (McCann et al., 2010) and duration of *Dictyostelium* aggregation $t_f^{exp} = 12h$.

In order to compute the final time of numerical integration t_f that corresponds to the finite duration of aggregation, we used the following relationship

obtained by dimensional analysis:

$$t_f = \frac{t_f^{exp} v^{exp}}{R_{eq}^{exp}} \frac{R_{eq}}{v_0} \approx 100 \tag{1}$$

Link between optimal velocity v_{opt} and adhesion force F_{adh}

Simulations of the self-propelled particles system suggest that v_{opt} and F_{adh} scale like:

$$v_{opt} = a\sqrt{F_{adh}} \tag{2}$$

where a is a constant (Fig. S6, white dotted line, and Fig. 7A, black line).

In order to understand such a relationship from a theoretical point of view , let us consider the collision between a self-propelled and a stationary particle (for instance, one that belongs to an aggregate – whose average speed is very small), as illustrated in Fig. S7. The equations of motion for each particle in the simulation are:

$$\frac{d\mathbf{r}_i(t)}{dt} = v_0\mathbf{n} + \mu\mathbf{F} \equiv \mathbf{v} \tag{3}$$

$$\frac{d\theta(t)}{dt} = \frac{1}{\tau} arcsin(\mathbf{n} \times \frac{\mathbf{v}}{v}) + \eta\xi_j(t) \tag{4}$$

where $\mathbf{r_i}$ is the position of particle i, v_0 its self-propelled speed, $\mathbf{n}$ a polarization unitary vector with angle θ, μ the mobility, τ is the characteristic time for the polarization to align in the scattering direction defined by $\mathbf{v}$, η is the noise intensity which defines a characteristic timescale $\tau_r \sim 1/\eta^2$ of the white rotational noise $\xi(t)$. For the analysis that follows, we consider a large value for the alignment and rotational characteristic times, so that the polarization direction (not the scattering direction) remains constant.

We want to estimate the duration of the contact between two particles when they encounter, that is the time they spend at a distance of less than the interaction range R_0. Comparison between this timescale and the timescale necessary for a particle to escape from an interaction will provide a scaling relation between the force intensity and the optimal velocity.

Consider a particle that is travelling with velocity $\mathbf{v}$ approaching the stationary particle. When the incident particle falls within the range R_0, one has to take into account the deviation in its trajectory that results from the attractive force. Since the force acts radially, we have to evaluate the velocity in the radial

direction (defined pointing outwards relative to the stationary particle) resulting from the self-propulsion and the action of the force. This is the projection in that direction of eq. 3:

$$v_r = v_0 \cos\alpha + \mu F_{adh}, \tag{5}$$

where α is the angle between the radial direction and the direction of the particle velocity (Fig. S7).

In the absence of angular noise, the incident particle will remain within the range of the force as long as the velocity in the outward radial direction is small enough to compensate the last term in eq. 5. The two particles detach when v_r is zero, which happens at a critical angle α^* where the components of the force and self-propulsion have opposite signs. That occurs when $\cos\alpha^* = \frac{\mu F_{adh}}{v_0}$ (Fig. S7). A small value for α^* implies a small value for the outward velocity component and, consequently, a longer contact time. We may then estimate the contact time as proportional to the attraction force range, R_0 and $\cos\alpha^*$ and inversely proportional to the speed, v_0, that is, $\tau_{ctc} \approx \frac{R_0 \cos\alpha^*}{v_0}$. From these relations, one obtains the following scaling:

$$\tau_{ctc} \approx \frac{R_0 \mu F_{adh}}{v_0^2} \tag{6}$$

The larger τ_{ctc}, the longer two particles remain attached.

For a given F_{adh}, let us consider a population of particles with high v_0 so that aggregation is limited by evaporation. Decreasing v_0 results in an increase in τ_{ctc}, particles thus escape at a lower rate and the fraction of aggregated particles increases. When $\tau_{ctc} > \tau$, however, whatever the speed, the incident particle will remain bound, as its self-propulsion will be quickly reoriented along a tangent direction. Once the particles enter such an 'orbit' upon contact, further increase in the contact time (corresponding to a decrease in v_0) has no effect. A decrease in the fraction of aggregated particles can nonetheless occur because of delayed aggregation, and more so, the slower are the particles. The optimal v_0 (*i.e.* v_{opt}) for which the fraction of aggregated particles is the highest is thus reached when $\tau_{ctc} = \tau$.

This condition yields:

$$v_{opt} = \frac{\sqrt{R_0 \mu F_{adh}}}{\tau} \tag{7}$$

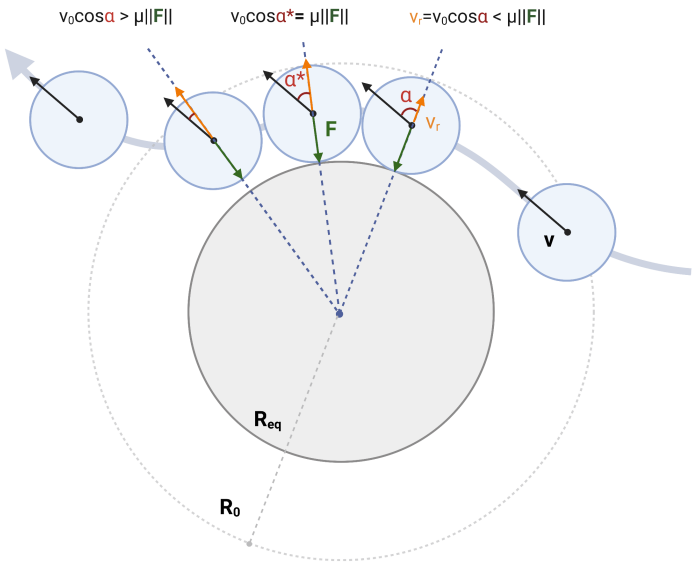

Figure S7: **Timing of particles interaction**. A self-propelled particle (blue, represented at successive times) comes into contact with a stationary particle (grey). The size of the stationary particle is enhanced for the sake of visualization. The alignment and rotational characteristic times are considered sufficiently large so that the polarization direction of the self-propelled particle remains constant during the encounter with the stationary one. The self-propelled particle detaches from the stationary particle when the projection of its self-propulsion in the direction connecting the particle centers is larger than the adhesive strength.

.

References

De Palo, G., Yi, D., Endres, R.G., 2017. A critical-like collective state leads to long-range cell communication in Dictyostelium discoideum aggregation. PLOS Biology 15, e1002602. doi:10.1371/journal.pbio.1002602.

Fily, Y., Marchetti, M.C., 2012. Athermal Phase Separation of Self-Propelled Particles with No Alignment. Physical Review Letters 108, 235702. doi:10.1103/PhysRevLett.108.235702.

McCann, C.P., Kriebel, P.W., Parent, C.A., Losert, W., 2010. Cell speed, persistence and information transmission during signal relay and collective migration. Journal of Cell Science 123, 1724–1731. doi:10.1242/jcs.060137.

Ostwald, W., 1896. Lehrbuch der allgemeinen chemie, vol. 2, part 1. engelmann, leipzig, germany.

Szabó, B., Szöllösi, G.J., Gönci, B., Jurányi, Z., Selmeczi, D., Vicsek, T., 2006. Phase transition in the collective migration of tissue cells: Experiment and model. Physical Review E 74, 061908. doi:10.1103/PhysRevE.74.061908.